# Cubesat Deployment from a Near Rectilinear Halo Orbit

Diane C. Davis[1]
*a.i. solutions, Houston, Texas, 77058, USA*

Emily M. Zimovan-Spreen[2]
*Johnson Space Center, Houston, Texas, 77058, USA*

Rolfe J. Power[3] and Kathleen C. Howell[4]
*Purdue University, West Lafayette, Indiana, 47907, USA*

**Satellites deployed from the Gateway in a Near Rectilinear Halo Orbit (NRHO) must be safely delivered to their desired destinations in cislunar space and beyond. The presence of simultaneously significant gravitational forces from the Moon, the Earth, and the Sun, along with the absence of atmospheric drag, complicates the mission design problem for cubesats deployed from the Gateway. The current investigation defines candidate green zones for safe satellite deployment, allowing a passive departing spacecraft to avoid recontact with the Gateway as it departs the NRHO vicinity.**

## I. Introduction

The Gateway [1] is proposed as an outpost in deep space: a proving ground for deep space technologies and a staging location for missions to the lunar surface and beyond Earth orbit. Missions commencing from the Gateway may include cubesats or other small satellites deployed to cislunar and deep space destinations. The deployment of a cubesat from the Gateway must consider the safety of the two spacecraft, ensuring that the small spacecraft does not threaten to collide with the Gateway as it departs the lunar vicinity. The initial deployment of the cubesat must result in a trajectory that naturally diverges from the Gateway without conjunction risk; the spacecraft may be passive due to design or contingencies. Understanding relative motion in the lunar vicinity is critically important for safe deployment of satellites from the Gateway.

The current baseline orbit for the Gateway is a Near Rectilinear Halo Orbit (NRHO) near the Moon [2]. With a period of approximately 6.56 days, the baseline NRHO exhibits a 9:2 resonance with the lunar synodic period, completing 9 revolutions around the Moon every 2 synodic months. The mean radius at perilune is approximately 3,400 km, while the orbit extends to a radius of approximately 71,000 km at apolune. This large orbit is significantly affected by the gravity of both the Earth and the Moon. The multibody nature of the dynamics in the NRHO vicinity can result in low-cost solutions for missions within and beyond cislunar space. However, designing a path that safely departs the Gateway is challenging for several reasons. First, the multibody regime is sensitive to small variations in the initial state so that changes to the magnitude, direction, or location of an initial separation maneuver result in significantly different outcomes; a large design space must be characterized to select a safe deployment maneuver. Second, the NRHO itself is a nearly stable orbit, and an object deployed with a small perturbation remains in the NRHO vicinity for several revolutions before departing. Finally, and most simply, in contrast to the low Earth orbit

[1] Principal Systems Engineer, a.i. solutions, Inc., diane.davis@ai-solutions.com, AIAA Associate Fellow.
[2] Aerospace Engineer, Flight Mechanics and Trajectory Design Branch, NASA Johnson Space Center, emily.m.spreen@nasa.gov.
[3] PhD Student, School of Aeronautics and Astronautics, Purdue University, rpower@purdue.edu, AIAA Student Member.
[4] Hsu Lo Distinguished Professor, School of Aeronautics and Astronautics, Purdue University, howell@purdue.edu, AIAA Fellow.

environment of the International Space Station (ISS), there is no atmospheric drag affecting the dynamics in the NRHO. Conversely, cubesats deployed from the ISS can avoid future conjunctions by deploying towards the Earth, where atmospheric drag ensures their orbits decay and do not encounter the ISS on later revolutions. By contrast, there is no immediately obvious direction to deploy from the Gateway in cislunar space to ensure safe departure. Thus, a broad design space is explored to determine safe deployment options for cubesats originating from the Gateway. The deployment strategy must consider the location along the NRHO for separation, the magnitude of the deployment velocity, and the direction of the perturbation.

Previous investigations [3, 4, 5] examined departure from the NRHO and escape from the Earth-Moon vicinity from the perspective of a logistics module (LM) or lunar lander ascent element (AE) disposal. Additional studies have explored the risk of recontact for spacecraft departing the Gateway [6], lunar impact trajectories originating from the Gateway NRHO [5, 7], and the cost of transfers from the Gateway NRHO to destinations in Sun-Earth halo orbits.[8] The current investigation extends these investigations with a focus on small satellite deployment. The analysis focuses on the safe deployment of cubesats from the Gateway while avoiding recontact risk, defining candidate green zones for departure from the Gateway in magnitude, direction, and location along the orbit.

## II. Background

### A. Cubesats and Deployers

Cubesats are of increasing interest in the space exploration domain, offering opportunities for science, education, technology demonstrations, and sensing. Over 850 cubesats had been launched by mid-2018, with 1000 expected to be launched by the end of 2021 [9]. Some cubesats are launched directly into orbit; others are deployed from the ISS or carried as comanifested missions with other spacecraft. While most cubesats to date have focused on explorations in Earth orbit, some have ventured beyond; as an example, the Mars Cube One (MarCo) probes traveled to Mars alongside the Mars Insight spacecraft in 2018 [10]. Multiple upcoming cubesat launches beyond Earth orbit focus on cislunar exploration; examples include the CAPSTONE mission expected to launch in March 2022 to a lunar NRHO [11], as well as eight of the 13 cubesats to be launched along with the Artemis I mission to the Moon [12]. Historically, the reliability of cubesats has been a concern. Although reliability is improving over time, by the end of 2018 only approximately 60% of cubesats had achieved mission success. Just over 20% of cubesats failed due to problems with the cubesats themselves [9].

Like the ISS, the Gateway offers a unique opportunity to enable cubesat deployment from an established base. In contrast to cubesats deployed from ISS, however, cubesats deployed from the Gateway may take advantage of originating in an NRHO to explore the lunar surface, cislunar space, or other destinations beyond Earth orbit. First, of course, a cubesat must be deployed, and specific deployment conditions are necessary to ensure the safety of both Gateway and the cubesat. If a cubesat is equipped with propulsive capability, the thrusters, communications, or other systems may not operate as expected. Thus, deployment must be designed such that a passive cubesat will depart the Gateway vicinity without threat of conjunction. In low Earth orbit, the presence of atmospheric drag ensures that a passive cubesat deployed towards the Earth will not have sufficient energy to recontact the ISS. In an NRHO, such a simple safe deployment option is not available. Many deployment mechanisms exist; however, a deployer for Gateway is not yet defined. In the current analysis, the deployer is assumed to be capable of ejecting the cubesat in a commanded direction with a specified $\Delta v$ magnitude between 0.5 m/s and 1.5 m/s. It is assumed that the timing of the deployment is accurate to within a few seconds, while acceptable error bounds on the magnitude and pointing of the deployment $\Delta v$ are assessed in this analysis.

### B. Dynamical Models

The current investigation employs two dynamical models to describe the motion of the Gateway and the deployed cubesats in space. The Circular Restricted 3-Body Problem effectively describes the behavior of objects in and near the Gateway NRHO in a simplified framework that enables pattern definition and an understanding of the underlying dynamical flow. Then, an N-body model based on ephemeris data provides higher-fidelity analysis that incorporates the eccentricity of the Earth and Moon as well as the effects of solar gravity, allowing assessment of trajectory consistency across epochs.

#### *1. The Circular Restricted 3-Body Problem*

The CR3BP describes the motion of a massless spacecraft affected by two primary gravitational bodies such as the Earth and the Moon. The model assumes that the two primary bodies are point masses orbiting their center of mass in circular orbits. The spacecraft moves freely under the influence of the two primaries, and its motion is described relative to a rotating reference frame. No closed-form solution exists to the CR3BP equations of motion, but five

equilibrium solutions, the libration points, are denoted $L_1$ through $L_5$. Stable and unstable periodic orbit families, including the $L_2$ halo orbits, emerge in the vicinity of the libration points. A single integral of the motion exists in the CR3BP, the Jacobi constant [5], written

$$J = 2U^* - v^2 \tag{1}$$

where $v$ is the rotating velocity magnitude. The pseudopotential $U^*$ is a function only of position, defined as

$$U^* = \frac{1}{2}(x^2 + y^2) + \frac{\mu}{r} + \frac{(1-\mu)}{d} \tag{2}$$

where $x$, $y$, and $z$ are components of the position vector relative to the barycenter in the Earth-Moon rotating frame and $\dot{x}$, $\dot{y}$, and $\dot{z}$ are components of the velocity vector in the same frame. The values $d$ and $r$ are the distances between the spacecraft and $P_1$ and $P_2$ respectively, and $\mu = \frac{m_2}{m_1+m_2}$ is the mass parameter of the system where $m_1$ and $m_2$ are the masses of the two primaries. For spacecraft orbiting in or near the Gateway NRHO, the Earth-Moon CR3BP delivers a good approximation for the trajectory and relative behaviors.

*2. The N-Body Ephemeris Model*

To confirm the CR3BP results in a higher-fidelity model, N-body differential equations and planetary ephemerides are employed. The N-body dynamics describe the motion of a spacecraft in an inertial frame relative to a central body under the gravitational influence of the central body and additional perturbing bodies. Within this analysis, the relative position of each perturbing body with respect to the central body is instantaneously computed by employing NAIF SPICE ephemeris data. The Moon is selected as the central body for numerical integration in the J2000 inertial frame. The Earth and Sun are included as point masses, and the Moon's gravity is modeled using the GRAIL (GRGM660PRIM) model truncated to degree and order 8. Solar radiation pressure (SRP) acting on a sphere is also included in the force model.

For multi-revolution propagations in the NRHO prior to a deployment maneuver, orbit maintenance maneuvers (OM maneuvers) are implemented [13]. Operational errors on the spacecraft are incorporated in the higher-fidelity modeling as gaussian errors with zero mean and 3σ values as follows. Each OM maneuver is associated with a navigation error on the spacecraft state of 1 km in position and 1 cm/s in velocity. Maneuver execution errors comprising 1.5% in magnitude and 1° in direction, as well as a fixed magnitude of 1.42 mm/s, are applied to each OM maneuver. Mismodeling in SRP assumptions provide 15% error in area and 30% error in coefficient of reflectivity. Momentum wheel desaturations are assumed to occur once per revolution near apolune with a translational $\Delta v$ component of 3 cm/s applied in a random direction. In some analyses, the deployment maneuver is applied including navigation errors and with execution errors in magnitude and direction as specified in each case.

**C. Gateway NRHO and Coordinate Definitions**

The Gateway NRHO is selected as the southern L2 halo orbit in the Earth-Moon system that exhibits a 9:2 resonance with the lunar synodic period. The resonant NRHO is favorable as a long-term orbit for the Gateway as it is nearly stable, and thus requires low orbit maintenance $\Delta v$, and also, when phased properly, excludes eclipses from the Earth's shadow. Perfectly periodic in the CR3BP, the NRHO exists as a quasi-periodic orbit in the higher-fidelity ephemeris model. A 15-year baseline trajectory is available on the JPL NAIF server [14]. The Gateway NRHO as computed in the CR3BP appears in an Earth-Moon rotating view in Fig. 1.

There are several ways to parameterize a location along the NRHO. One parameter used in the current study is osculating true anomaly, TA, as pictured in Fig. 1(a). Describing locations along the NRHO in terms of TA is useful since it is an intuitive measure familiar from Keplerian dynamics. In some visualizations, however, parametrizing the NRHO by TA can be somewhat misleading since the spacecraft moves very quickly through TA near the Moon. While the period of the orbit is 6.56 days, a spacecraft in the NRHO moves from TA = 0° at perilune to TA = 120° in just 3.2 hours. A second method to parameterize the NRHO is by mean anomaly, or, equivalently, by time, as in Fig. 1(b). This measure of location along the NRHO is advantageous as operational planning and execution times are considered. However, it suffers from the opposite challenge seen with true anomaly. Namely, a spacecraft in the NRHO moves quickly near perilune and quite slowly near apolune, so that points spaced equally in time are clustered near apolune, while points spaced equally in TA are clustered near perilune. To address this challenge, another useful angle is also employed in this investigation: osculating eccentric anomaly (EA), as illustrated in Fig. 1(c). While EA has the disadvantage of requiring the solution to Kepler's equation, it is more evenly distributed around the NRHO, reaching a value of only 45° after 3.2 hours of flight, and achieving a value of 90° a full 16 hours past perilune.

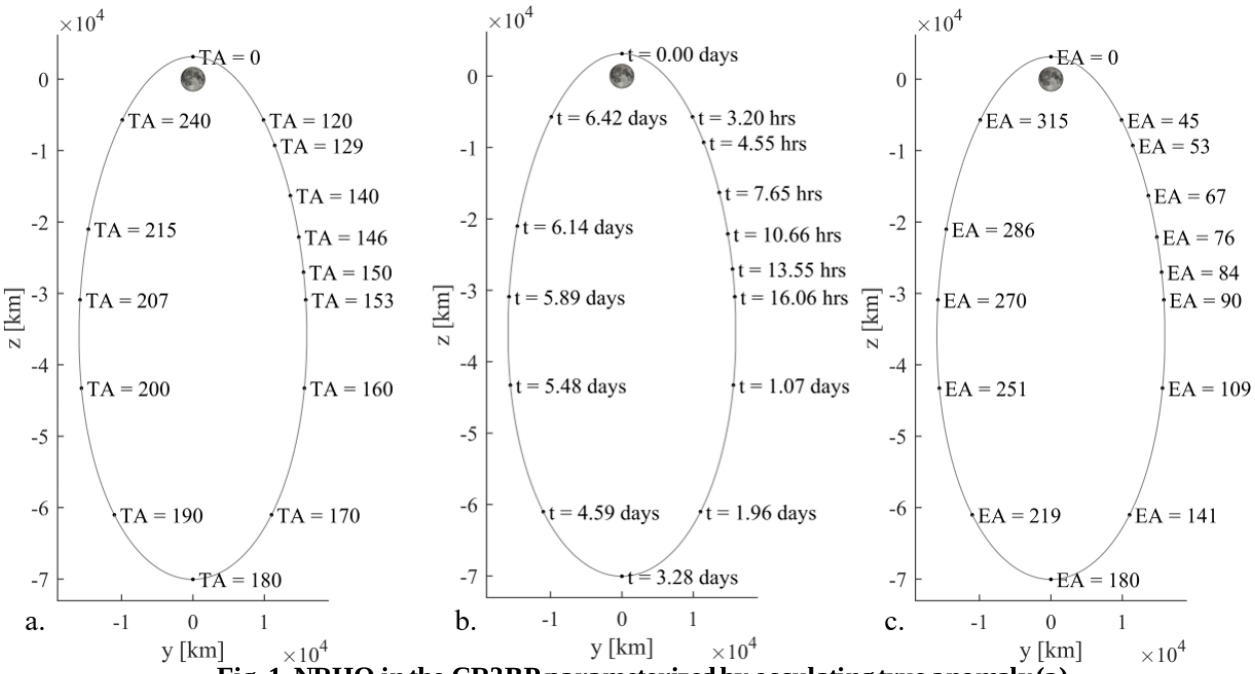


**Fig. 1. NRHO in the CR3BP parameterized by osculating true anomaly (a), time past perilune (b), and osculating eccentric anomaly (c).**

Multiple options are available for describing maneuver direction, and the current investigation employs two. In some applications, it is simplest to describe a burn direction in the Velocity-Normal-Binormal (VNB) frame. The VNB directions are defined along the orbit such that the V direction aligns with the rotating velocity, $V = (\dot{x}, \dot{y}, \dot{z})$, the N direction corresponds to the orbit normal, $N = (x, y, z) \times (\dot{x}, \dot{y}, \dot{z})$, and B completes the right handed system. For other applications, it is simpler to use two parameters to describe the burn direction, yaw and pitch. The yaw angle ranges from -180° to 180° in the V-N plane, and the pitch angle ranges from -90° to 90° out of the V-N plane. Both maneuver direction options are available in the CR3BP and ephemeris model analyses.

## III. Departure, Recontacts, and Range

When a cubesat is deployed from the Gateway, the maneuver size, location, and direction determine its post-maneuver behavior. For the small $\Delta v$ magnitudes between 0.5 and 1.5 m/s in the current study, a cubesat remains near the NRHO for several revolutions before it departs the lunar vicinity. While the cubesat remains in close proximity to the Moon, there is a risk of recontact with the Gateway. To bound the problem, the concepts of NRHO departure and recontact are defined. Then, the range between the Gateway and the deployed cubesats is explored to characterize desirable and undesirable cubesat behavior.

To define departure from the NRHO, a momentum integral is employed [3,15]. The momentum integral, MI, is a line integral of the position vector from the initial time, $t_0$, to the current time, $t$,

$$\mathrm{MI}(t) = \int_{t_0}^{t} x(\tau)\dot{x}(\tau) + y(\tau)\dot{y}(\tau) + z(\tau)\dot{z}(\tau)\, d\tau \tag{1}$$

For a perfectly periodic halo orbit in the CR3BP, the MI is also periodic and returns to zero after each period. In the higher-fidelity ephemeris model, the value of the MI does not return precisely to zero over one period; however, it does remain bounded while the spacecraft remains in the NRHO. Over time, as the orbit of a perturbed spacecraft diverges from the NRHO, the MI also diverges, and departure is defined in terms of the divergence of the MI. When the magnitude of the MI crosses a particular threshold, the debris object is considered "departed" from the NRHO. The specific value of the MI threshold depends on the application; in the current study, values of 0.1 and 0.2 are selected for various applications.

After a cubesat has separated from the Gateway but prior to its departure from the vicinity of the NRHO, recontact with the Gateway is a risk. In the current study, a cubesat trajectory is considered a recontact risk if, after initial departure from a 100 km keep-out sphere, the cubesat re-enters the keep-out sphere with decreasing range. For a

cubesat departing the Gateway, risk of recontact is assessed while the separated object remains nearby the NRHO; after departure, the risk of immediate recontact is assumed to cease. In reality, return to the vicinity of the NRHO after initial departure is also a concern; however, this analysis is reserved for a future investigation. To assess this risk of recontact, the range between the Gateway and the departing object is computed for various departure maneuvers. The range between the cubesat and the Gateway follows a pattern based on the location, magnitude, and direction of the deployment $\Delta v$. Certain patterns are desirable for designing a safe cubesat deployment, while others must be avoided to ensure safe departure from the lunar vicinity. Range plots for three sample departures appear in Fig. 2. The horizontal axis represents time past deployment, while the vertical axis denotes the range between Gateway and the deployed cubesat. The green curve represents a cubesat that departs safely from the Gateway. Deployed at TA = 140° (EA = 67°) with $\Delta v$ = 1.2 m/s in a direction that encourages fast departure, the range increases over time until it reaches an initial peak at perilune 6.4 days after deployment. The range then decreases to just under 2,000 km at apolune. The pattern repeats, with increasing range at subsequent perilunes. The MI threshold of 0.2 is crossed approximately 43 days after deployment, and the cubesat departs the NRHO vicinity without conjunction risk. Two unfavorable behaviors are also represented in the plot. The first is demonstrated by the blue curve. In this case, the cubesat is again deployed with $\Delta v$ = 1.2 m/s in a particular direction, but in this case, it is deployed slightly later, at TA = 160° (EA = 109°). For the first 45 days after deployment, the range plot follows a pattern very similar to the favorable departure highlighted in green. However, in this case, the MI threshold is not reached, and the spacecraft does not quickly depart the lunar vicinity. It remains in a chaotic orbit near the Moon for approximately 110 days prior to departure. While this specific example does not experience a conjunction, in the presence of deployment errors, the unpredictable behavior post-deployment can lead to recontact risk and should be avoided. A second undesirable case appears in red. Here, the cubesat is deployed with $\Delta v$ = 1.2 m/s at TA = 175° (EA = 160°). As before, for the first several revolutions, the range increases at perilune as desired. However, about 30 days after deployment, the range dips sharply, and the two spacecraft experience a close approach as they pass simultaneously through perilune. This flip in the range pattern at perilune leads to a conjunction risk.

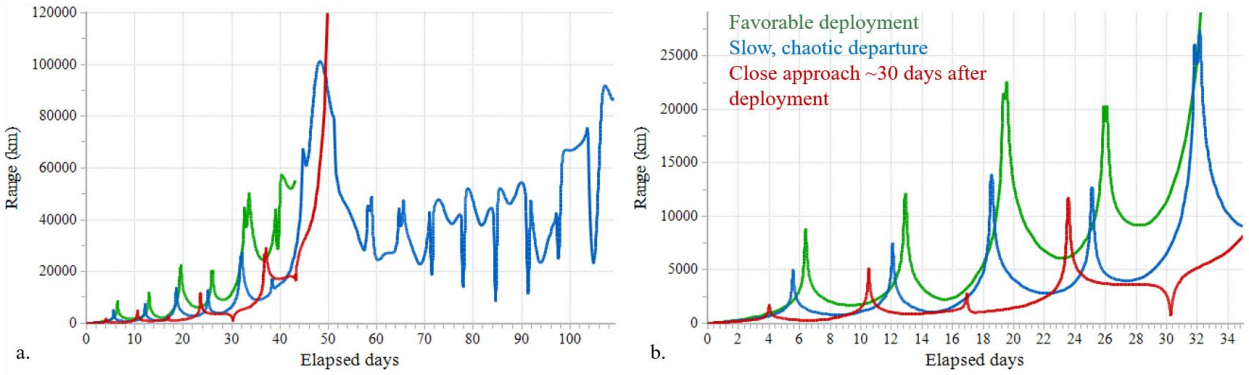


**Fig. 2. Gateway-cubesat range over time for three deployment cases in the ephemeris model. Full view (a) and zoomed view (b).**

In summary, the two undesirable patterns in the range plots must be avoided to ensure safe cubesat deployment. First, slow departures that result in chaotic long-term loitering near the Moon lead to conjunction risk; a fast, reliable departure is necessary. Second, flips in the range plots that represent close approaches at perilune lead to serious risks of recontact. Departing cubesats must reach maxima in range from Gateway at each perilune passage throughout their departure from NRHO. In each case, the undesirable behavior leading to recontact risk must be avoided in the presence of deployment errors in magnitude and direction. Finally, the desirable behavior must be consistent in the ephemeris model regardless of deployment epoch. The goal of the current analysis is to define a green zone for cubesat deployment; that is, a range of values of TA along the NRHO and specific magnitudes and directions of deployment $\Delta v$ that consistently achieve safe, reliable departure from the NRHO in the presence of deployment errors and across deployment epochs.

## IV. Deployment Maneuver Directions

The post-deployment behavior of a departing cubesat is highly sensitive to the direction of the deployment $\Delta v$. Phillips and Davis [6] highlight the extensive scope of the design space when all possible maneuver directions are considered and introduce recontact maps to manage the resulting data. Davis et al. [4] note the patterns apparent in

post-deployment trajectory behavior when the $\Delta v$ is assessed in the VNB frame and focus the analysis on velocity-direction maneuvers. In the current investigation, the Cauchy-Green strain tensor (CGT) [15, 16] is employed to compute maneuver directions that yield the greatest separation between the two spacecraft after selected time horizons. The CGT, $C$, is computed from the state transition matrix (STM), $\Phi$. The STM maps an initial perturbation along a reference path to the final perturbation after a given time horizon such that

$$\delta \mathrm{x}(t_f) = \Phi(t_f, t_0)\delta \mathrm{x}(t_0) \tag{2}$$

where the initial and final epochs are represented by $t_0$ and $t_f$ respectively. Squaring the perturbation at the final state yields

$$\left\|\delta \mathrm{x}(t_f)\right\|^2 = \delta \mathrm{x}(t_0)^T C(t_f, t_0)\delta \mathrm{x}(t_0) \tag{3}$$

where the CGT is computed from the STM as

$$C(t_f, t_0) = \Phi^T(t_f, t_0)\Phi(t_f, t_0) \tag{4}$$

The positive-definite CGT then describes the stretching of the flow in the vicinity of the reference trajectory. An eigen-decomposition of the time-dependent CGT yields the direction of a perturbation that results in the largest divergence from the reference after a given time horizon, denoted the most-stretching direction, as well as the direction of perturbation than yields the smallest departure from the reference after the specified time horizon, i.e, the most-restoring direction. In the current analysis, the goal is to identify the velocity perturbation that yields the largest separation in position within a given time horizon. Thus, considering the submatrices of the STM,

$$\Phi(t_f, t_0) = \begin{vmatrix} \phi_{rr} & \phi_{rv} \\ \phi_{vr} & \phi_{vv} \end{vmatrix} \tag{5}$$

the upper right-hand submatrix, $\phi_{rv}$, maps an initial velocity perturbation to a final position separation. The most-stretching direction associated with this mapping is achieved by taking the maximum singular values of the $\phi_{rv}$ submatrix for a specified time horizon. Further details appear in Muralidharan and Howell [16].

The most-stretching direction associated with the CGT depends on a starting location for the perturbation along the NRHO as well as the time horizon selected for the analysis. For example, the VNB components of the most-stretching directions computed in the CR3BP at TA = 150° (EA = 84°) and TA = EA = 180° appear in Fig. 3 for time horizons ranging from zero to ten revolutions within the NRHO. Since these directions are vectors, the most-stretching direction exists in both a positive and negative sense. In both cases, it is apparent that the most-stretching direction changes as the time horizon varies. That is, a maneuver that yields a significant separation between the Gateway and a deployed cubesat after 1.5 revolutions may not be oriented in the best direction to achieve a desirable separation after 6.5 revolutions, for example. The large variations in most stretching direction are particularly notable for departures near apolune, as in Fig. 3(b). It is also notable from the plots in Fig. 3 that the perturbation directions that lead to large separation downstream change significantly from one location along the NRHO to another.

With the computation of the most-stretching directions at varying time horizons complete, their effectiveness as maneuver directions is assessed. First, a deployment location along the NRHO is selected. Then, a deployment maneuver with a magnitude of 1 m/s is simulated in 100 directions evenly distributed around a sphere. After each maneuver, the range between the Gateway and the cubesat is computed for 5.5 revolutions of the Gateway within the NRHO. The resulting range is plotted in grey as a function of time for deployment at TA = 150° (EA = 84°) in Fig. 4 and for deployment at TA = EA = 180° in Fig. 5. Then, the range resulting from deployment in the most-stretching direction for a selected time horizon is overlaid in red, while the range resulting from a deployment maneuver in the most-restoring direction for a selected time horizon is plotted in blue. For example, consider the range plots in Fig. 4(a). The grey lines represent the range resulting from 1 m/s maneuvers evenly spaced in direction around a sphere. The vertical dashed line denotes a 0.5 revolution time horizon. The red curve represents the range over time between the Gateway and a cubesat deployed in the most-stretching direction with a 0.5-revolution time horizon. Note that 0.5 revolutions after deployment, the most-stretching direction does, in fact, yield the trajectory that has achieved the largest separation from the Gateway. Conversely, the blue line is generated by a cubesat deployed in the most-restoring direction with a 0.5-revolution time horizon. One half revolution after the deployment maneuver, the cubesat deployed in the most-restoring direction remains closest to the Gateway. Note, however, in Fig. 4(a) there are grey lines that remain closer to the Gateway for propagation times greater than 0.5 revolutions. In Fig. 4(b), the most-stretching and most-restoring directions with a 1-revolution time horizon are plotted in red and blue respectively. One revolution

after deployment, as denoted by the vertical black dotted line, the most-stretching and most-restoring directions do indeed yield the trajectories that are farthest and closest, respectively, to the Gateway. As the horizon time is increased to 1.5 revolutions and 2 revolutions in Fig. 4(c) and Fig. 4(d), the most-stretching and most-restoring directions continue to bound the range plots across all maneuver directions.

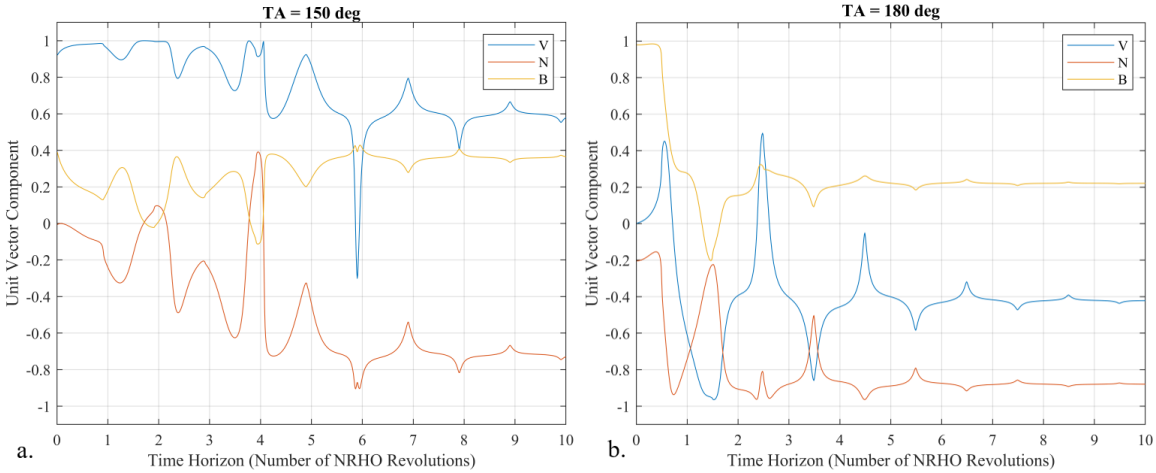


**Fig. 3. VNB components of the most-stretching directions as a function of time horizon for TA = 150° (a) and TA = 180° (b) in the CR3BP.**

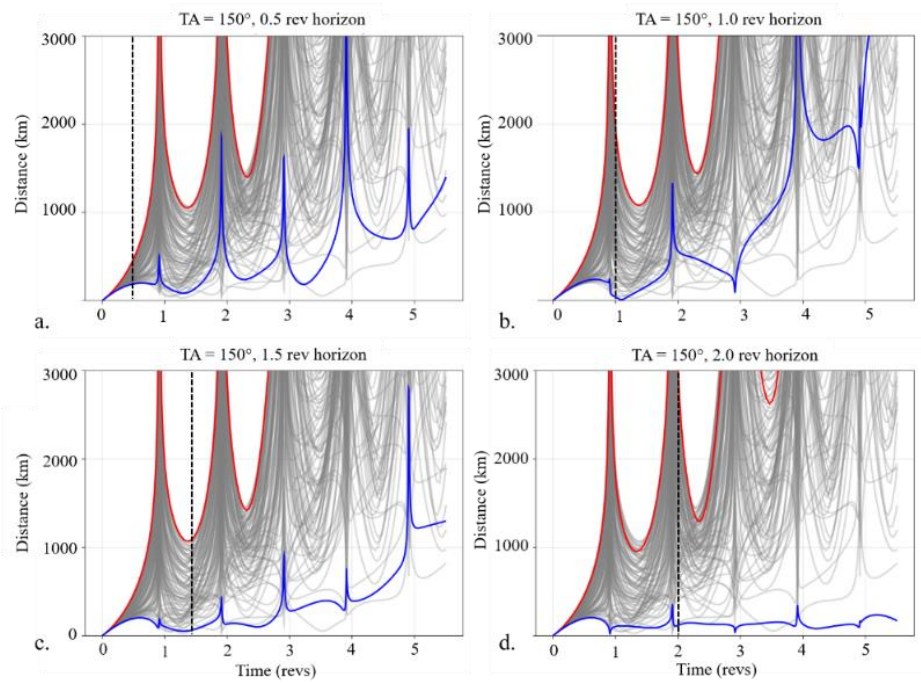


**Fig. 4. Gateway-cubesat range as a function of time past deployment for all directions at TA = 150° or EA = 84° in the CR3BP. Most-stretching (red) and most-restoring (blue) directions plotted for four time horizons.**

A similar set of plots is generated for deployment maneuvers at apolune, or TA = EA = 180°. These plots appear in Fig. 5. As before, at each of the four time horizons represented in Fig. 5, the red curve, representing a trajectory resulting from deployment in the most-stretching direction, bounds the upper limit of the range at the dotted line representing the time horizon. Similarly, the maneuver in the most-restoring direction generates the blue curve, which bounds the Gateway-cubesat range on the lower side at the given time horizon. However, it is important to note that for deployment at TA = 180°, the most-stretching direction at a time horizon of 0.5 revolutions, for example, plotted

in red in Fig. 5(a), results in a close approach approximately 3.5 revolutions downstream. Similarly, the blue curve in Fig. 5(c) is generated by a maneuver in the most-restoring direction with a 1.5 revolution time horizon. This maneuver behaves as expected, yielding the trajectory with the closest proximity to Gateway at the dotted line. However, about one revolution later, the same blue trajectory has diverged significantly from the Gateway trajectory. In short, in each of the range plots in Fig. 5, the most-stretching and most-restoring directions bound the range at the specific time horizon, but the behavior is specific to the selected propagation time and does not hold across all time. This result is consistent with the large variations in stretching direction as the horizon time varies, as noted in Fig. 3(b).

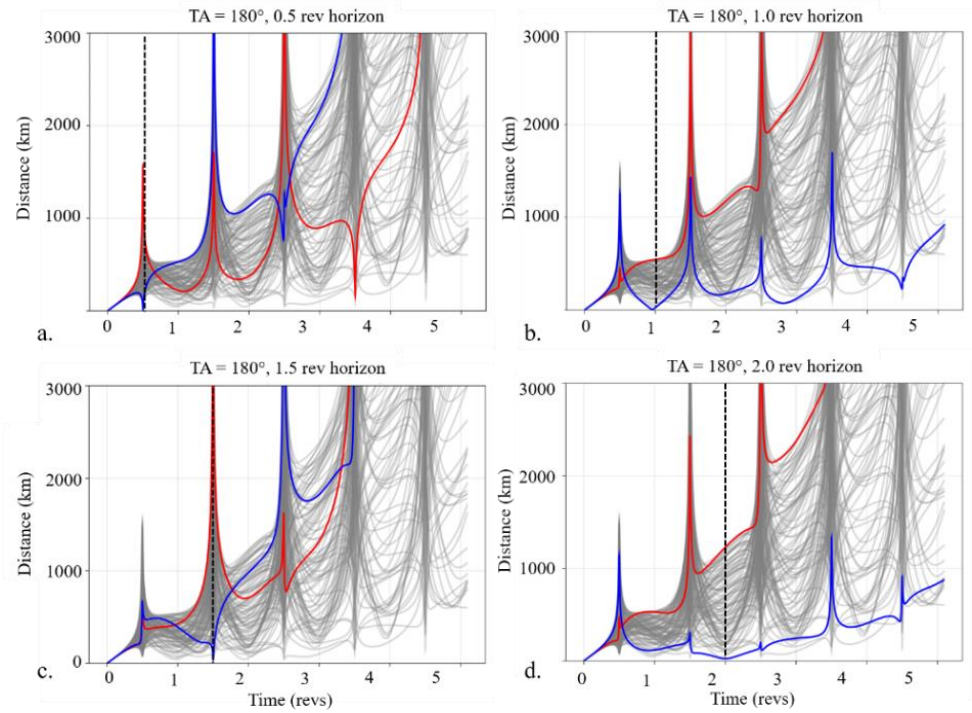


**Fig. 5. Gateway-cubesat range as a function of time past deployment for all directions at TA = EA = 180° in the CR3BP. Most-stretching (red) and most-restoring (blue) directions plotted for four time horizons.**

In Fig. 3, the most-stretching direction is investigated across a range of time horizons at two locations along the NRHO: TA = 150° (EA = 84°) and TA = EA = 180°. Conversely, in Fig. 6, the stretching directions are plotted as functions of TA, EA, and time past perilune for two selected time horizons, 1.5 revolutions and 6.5 revolutions. In Fig. 6(a) - Fig. 6(c), the most-stretching directions are plotted in terms of yaw and pitch relative to the velocity vector, while in Fig. 6(d) -Fig. 6(f), the same stretching directions appear in VNB coordinates. Perilune, corresponding to TA = EA = 0° and $t = 0$, is centered in each plot. It is immediately apparent that the most-stretching direction is aligned with the velocity vector near perilune. Additionally, the 1.5 and 6.5 revolution time horizons yield very similar stretching directions near perilune, and very distinct directions near apolune, at the edges of the plots. Note that the eigenvector that yields the most-stretching direction can be applied in either a positive or negative sense. In the current study, the "positive" stretching direction is selected, defined such that the $\Delta v$ perturbation decreases Jacobi constant, increasing the energy of the trajectory.

The stretching directions are plotted relative to three measures of location along the NRHO in Fig. 6 to illustrate the challenges or benefits associated with each. The left-hand column of Fig. 6, with directions plotted against TA, focuses attention on the region near perilune, where TA changes quickly. Recall that a spacecraft in an NRHO spends just 3.2 hours of its 6.56-day period in the span $0° < TA < 120°$. Thus, the majority of the plot describes only a few hours of time within the NRHO, and the stretching directions appear to change very slowly near perilune and quickly near apolune. The right-hand column of Fig. 6, on the other hand, shows the stretching directions as a function of time past perilune. Since the spacecraft moves slowly near apolune, the directions plotted as functions of time reflect the changes in direction a spacecraft would experience in flight: fast changes in stretching direction as the spacecraft speeds past the Moon, and slow changes while far from the Moon. The center column of Fig. 6, showing the stretching directions plotted against EA, represents a more even distribution of points around the NRHO, and provides a view less focused on behavior at either perilune or apolune.

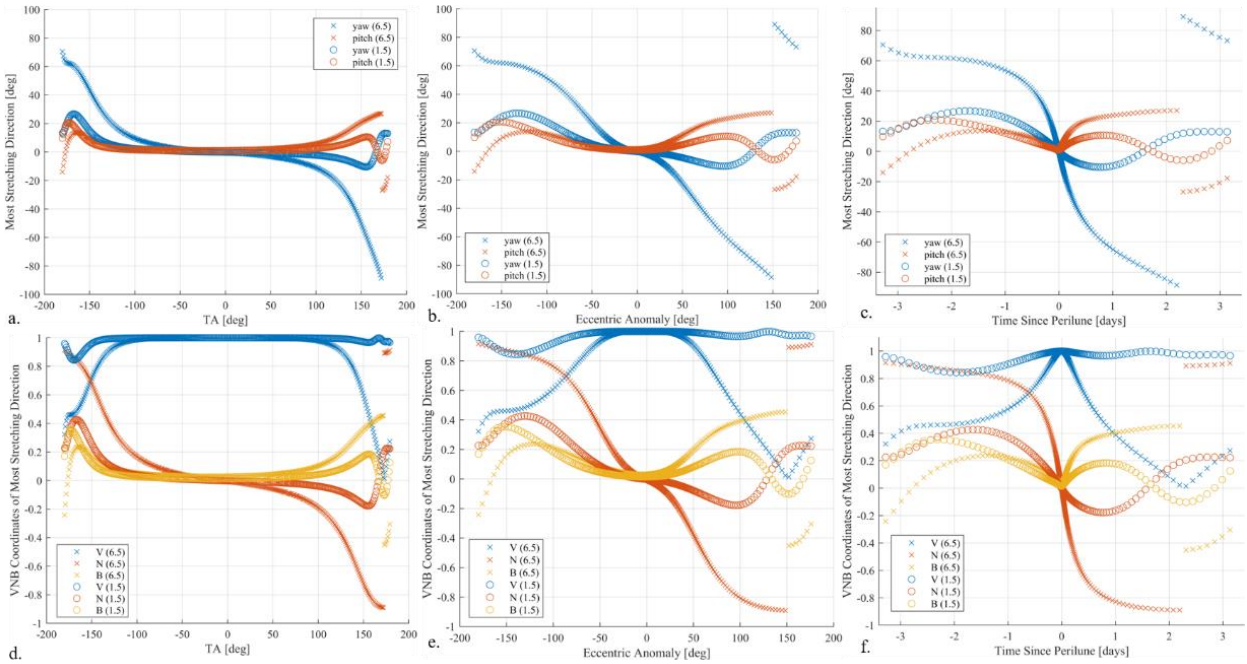


**Fig. 6. Stretching directions for 1.5 and 6.5 rev time horizons for deployment locations around the NRHO in the CR3BP. Yaw and pitch coordinates (a) and VNB coordinates (b).**

With the stretching directions defined for a variety of time horizons, post-deployment trajectory behavior is considered to select the specific time horizons for use in the search for a cubesat deployment green zone. As illustrated in Fig. 2, two desired behaviors are identified for safe deployment. First, the cubesat must avoid conjunctions with the Gateway over its first several revolutions. Then, the cubesat must depart the NRHO vicinity quickly. To select a time horizon to satisfy the first of these behaviors, a histogram of recontacts as a function of propagation time is generated for each of the grey curves in Fig. 4. The recontact histogram appears in Fig. 7(a) for the 100 trajectories deployed with a magnitude of 1 m/s from TA = 150° (EA = 84°) in evenly spaced directions around a sphere. The majority of recontacts occur approximately 1.5 revolutions after deployment, with over 90% of recontacts occurring prior to completing 3 revolutions after deployment. The mean and median recontact times appear as a function of TA in Fig. 7(b). For deployments such that 120° < TA < 160°, both the mean and median recontact times remain below 2 revolutions. Thus, to avoid recontact in the first several revolutions prior to NRHO departure, the most-stretching direction with a time horizon of 1.5 revolutions is selected as a candidate deployment direction.

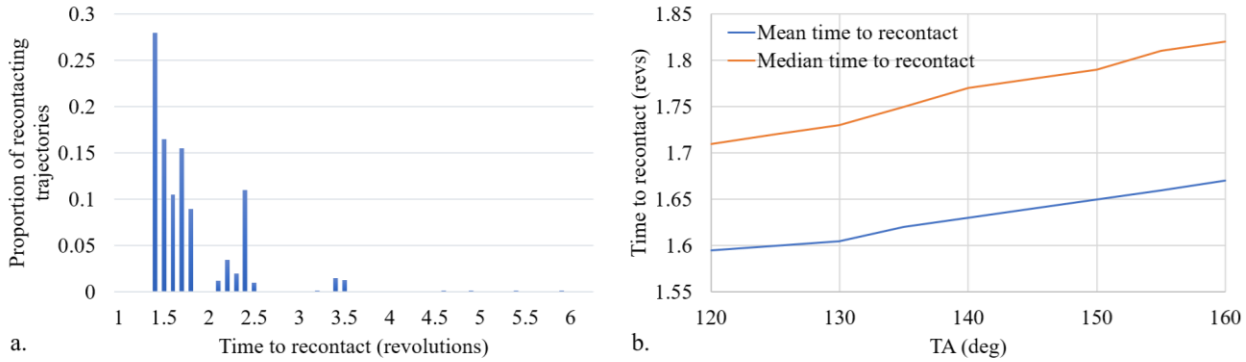


**Fig. 7. Histogram of recontact time for deployment in all directions from TA = 150° (EA = 84°) (a). Mean and median recontact times for deployment in all directions from 120° < TA < 160° (b).**

The second desired behavior is a fast departure from the NRHO vicinity that avoids chaotic long-term trajectories near the Moon. As a baseline, a histogram is generated representing time to depart for 100 trajectories generated from a 1 m/s deployment at TA = 150° (EA = 84°) in directions equally spaced around a sphere. This histogram appears in Fig. 8. The majority of departures occur for propagation times shorter than 8 revolutions in duration. Additionally, the shortest departures are observed to occur within a propagation time of approximately 6.5 revolutions. With the goal

of departing the NRHO as quickly as possible, the most-stretching direction with a time horizon of 6.5 revolutions is selected as a second candidate deployment direction.

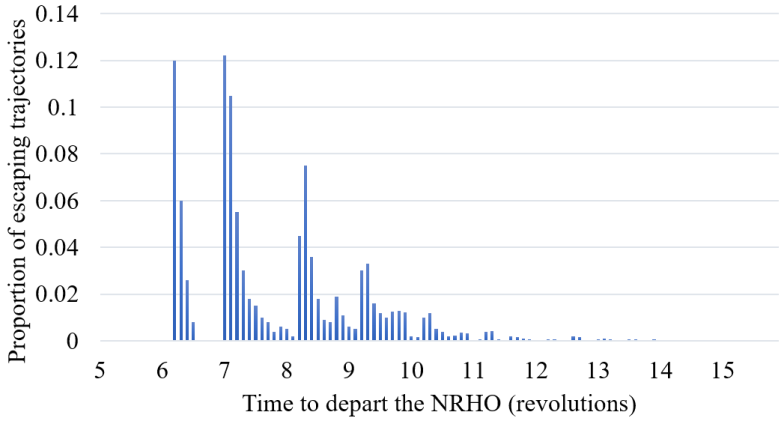


**Fig. 8. Histogram of time to depart the NRHO for deployment in all directions from TA = 150° (EA = 84°) in the CR3BP.**

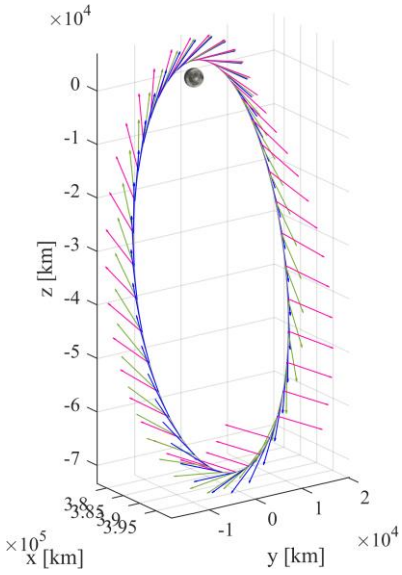


**Fig. 9. Stretching directions for a 1.5 (green) and 6.5 (pink) revolution time horizon, and the velocity direction (blue) plotted around the NRHO.**

The directions associated with the two candidate time horizons for cubesat deployment appear plotted around the CR3BP NRHO in Fig. 9. The green arrows represent the stretching direction with a 1.5 revolution time horizon as the NRHO evolves in true anomaly, while the 6.5 revolution time horizon stretching direction is marked by pink arrows around the NRHO. In addition, the velocity direction, a focus of previous investigations, appears as a set of blue arrows. The green arrows, thus, mark the direction of deployment selected to help the cubesat avoid short-term conjunctions with the Gateway, while the pink arrows signify deployment directions designed to enable fast departure from the NRHO vicinity. The three directions align well near perilune, as illustrated in Fig. 6, but the stretching directions differ from each other and from the velocity direction for locations along the NRHO away from perilune.

## V. Deployment Locations Along the NRHO

With two candidate deployment directions defined, a next step is determining where along the NRHO to release a cubesat. Deployments near perilune are immediately ruled out for several reasons. First, in the vicinity of the Moon, the dynamics in the NRHO are very sensitive. This sensitivity suggests that any errors in timing, magnitude, and direction are magnified for deployment in the vicinity of perilune [4]. Additionally, perturbations to the Gateway resulting from cubesat deployment near perilune are more expensive to mitigate as Gateway performs orbit maintenance in the NRHO [17]. Second, orbit determination errors are significantly larger near perilune in an NRHO [17,18]. That is, the Gateway's position and velocity state is less well known in the perilune vicinity, so maneuver execution errors are unavoidably larger if deployment occurs near perilune. Finally, when Gateway construction is complete, the spacecraft is expected to experience large gravity gradient torques near the Moon that will require active attitude control via attitude control thrusters [19]. As a result of perturbations associated with the active attitude control activity, deployment in the lunar vicinity will be associated with larger execution errors, or may, in fact, be infeasible. A keep-out zone for deployment is thus delineated in the perilune vicinity, defined as -120° < TA < 120°, or, equivalently, -45° < EA < 45°, or within approximately 3.2 hours of perilune. This keep-out zone includes the portions of the NRHO that fall within a 10,000 km radius of the Moon.

The next goal is to exclude regions along the NRHO where deployment leads to close approaches at perilune passages, as illustrated by the red curve in Fig. 2. With a focus on two selected deployment directions, the most-stretching directions after 1.5-revolution and 6.5-revolution time horizons, the deployment locations that result in close perilune approaches are detectable in Fig. 10. The colormaps in Fig. 10 represent the Gateway-cubesat range as a function of EA at deployment (vertical axes) and time since deployment (horizontal axes) as computed in the CR3BP.

Shades of blue represent smaller range values, while shades of yellow represent larger ranges. The plots span the first 55 days after deployment. Fig. 10a corresponds to deployment in the 1.5-revolution stretching direction, while Fig. 10(b) characterizes deployment in the 6.5-revolution stretching direction. A discontinuity in Fig. 10(b) at EA = 153° (TA = 173°) is the result of a sign change in the most-stretching direction that ensures the maneuver increases the cubesat energy, or decreases the value of Jacobi constant. Apolune is marked by horizontal dotted lines, while perilune deployments exist at the top and bottom boundaries of the plots. A region of fast departures is visible as a patch of bright yellow signifying distant range in the upper and lower right-hand corners of each plot, though both of these regions lie within the perilune keep-out zone where deployment is not permitted. Maneuver locations resulting in slow departures are marked in Fig. 10(a), visible by the blue shades representing small Gateway-cubesat range that extend through 55 days after deployment. The perilune passages are visible as bright vertical lines in the colormaps, as marked by black arrows in Fig. 10(a). Note, however, that for some deployment locations along the NRHO, the bright line representing perilune turns dark blue. Examples are circled in black in Fig. 10. These dark blue regions represent low values of Gateway-cubesat range at perilune and correspond to the undesirable close approaches at perilune that must be avoided. Clearly, the close approaches follow deployment maneuvers located within particular, predictable locations along the NRHO. These EA ranges are bounded by solid black horizontal lines in Fig. 10. The locations along the NRHO that result in close approaches at perilune are visualized along the NRHO in Fig. 11. For deployment in the most-stretching direction associated with a 1.5-revolution time horizon, a single region comprising approximately 2.5 days near apolune is excluded to avoid close approaches. This region, spanning 175° < TA < 195° or, equivalently, 160° < EA < 236°, is highlighted in light red in Fig. 11(a), along with the perilune keep-out region marked in bright red. For a cubesat deployment in the 6.5-revolution most-stretching direction, two regions emerge, one on either side of apolune, that yield undesirable close approaches. These are depicted in Fig. 11(b) in dark red. The region before apolune comprises 154° < TA < 173°, or 93° < EA < 152°. After apolune, the keep-out region is defined by 187° < TA < 207°, or 208° < EA < 269°. By avoiding the regions marked in red in Fig. 11, a cubesat avoids the effects of sensitivity near perilune as well as close approaches at perilune passage several revolutions after deployment. These CR3BP results are confirmed via spot checks in the ephemeris model.

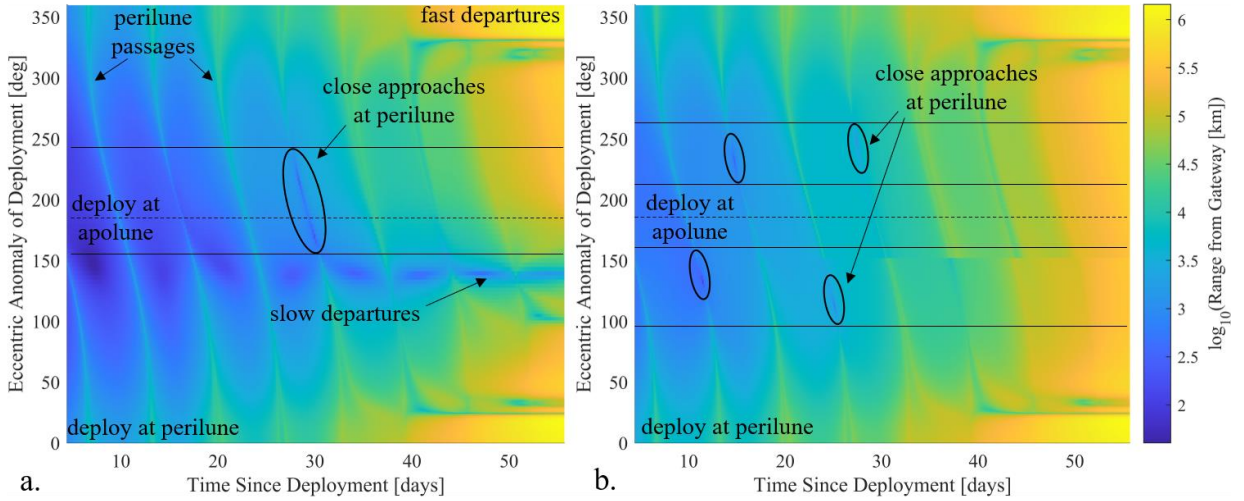


**Fig. 10. Gateway-cubesat range as a function of deployment EA and time past deployment in the CR3BP. Deployment in the most-stretching directions after 1.5 revolution time horizon (a) and 6.5 revolution time horizon (b) with a 1 m/s $\Delta v$.**

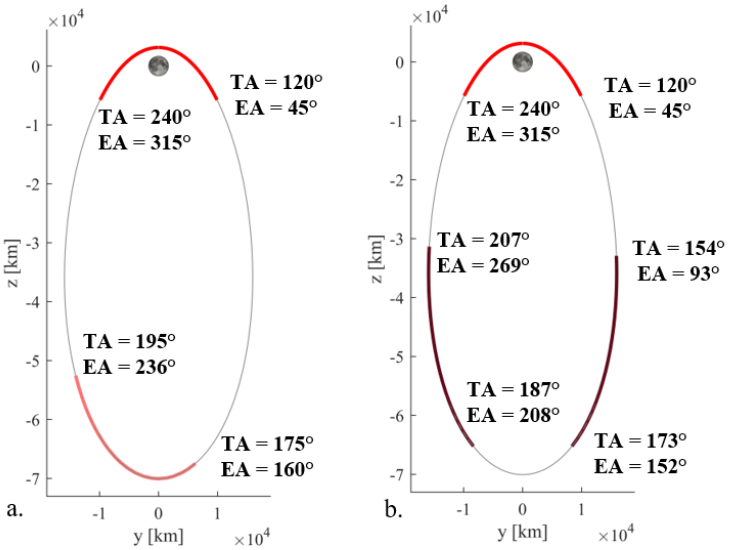


**Fig. 11. Keep-out regions for deployment in the most-stretching directions after a 1.5 revolution time horizon (a) and a 6.5 revolution time horizon (b).**

A third goal when deploying a cubesat is to avoid regions along the NRHO that lead to long-duration stays in the lunar vicinity. Analysis is first completed in the CR3BP. A broad overview of the design space is available by displaying the momentum integral MI as a function of deployment location (EA) and elapsed time after deployment. For example, the plots in Fig. 12(a) and Fig. 12(b) are generated by 1 m/s deployment maneuvers distributed around the NRHO in the 1.5-revolution stretching direction and the 6.5-revolution stretching direction, respectively. The plots are colored according to the magnitude of MI over time. Shades of blue represent small values of MI magnitude, or states in close proximity to the NRHO, while shades of yellow appear for large magnitudes of MI, or states that have diverged significantly from the NRHO. At the maximum value of MI = 0.2, the cubesat is considered departed from the NRHO. It is immediately apparent that deployment at some values of EA results in fast departures from the NRHO, in as little as 40 days. For other deployment locations, the cubesat has not formally departed the NRHO after 55 days. The locations along the NRHO that quickly reach the threshold at MI = 0.2 are desirable for deployment, while those deployment locations that do not achieve NRHO departure after 55 days should be avoided. Note that more of the EA values along the NRHO achieve fast departure for deployment in the 6.5-revolution stretching direction in Fig. 12(b) as compared to the 1.5-revolution stretching direction in Fig. 12(a). This result is intuitive given the 6.5 stretching direction is included with the goal of facilitating faster NRHO departures.

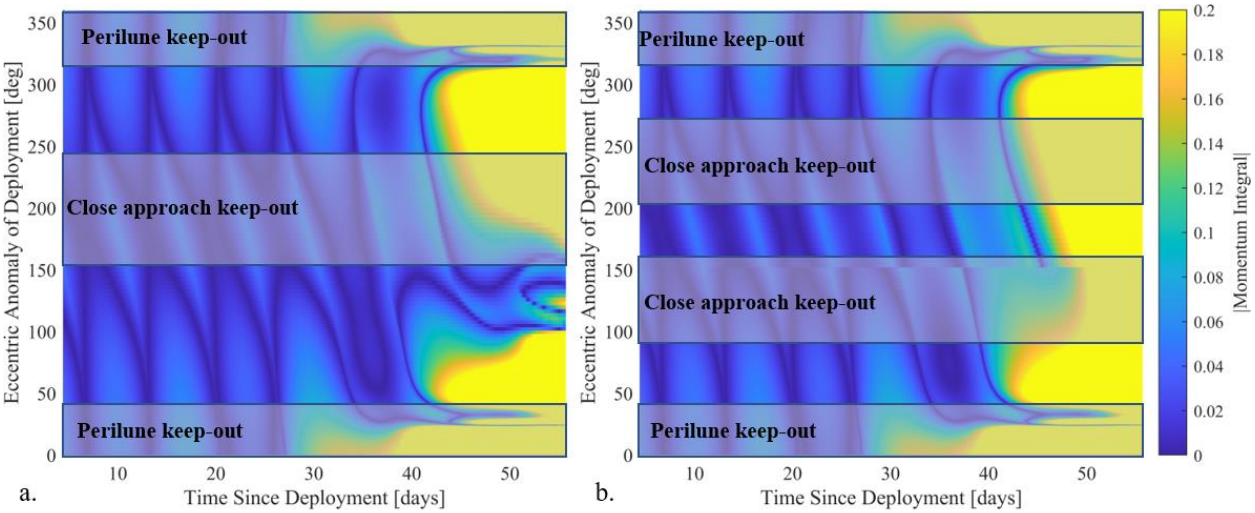


**Fig. 12. Momentum integral as a function of deployment EA and time past deployment in the CR3BP. Deployment in the most-stretching directions after 1.5 revolution time horizon (a) and 6.5 revolution time horizon (b) with a 1 m/s $\Delta v$.**

In Fig. 12, the MI plots are overlaid with the keep-out regions associated with perilune deployments and with close approaches at subsequent perilune passages. The remaining regions that quickly achieve the threshold magnitude of MI = 0.2, i.e., those EA values reaching shades of yellow, both avoid close approaches and quickly depart the NRHO. To better illustrate the conclusions from Fig. 12, plots of the Gateway-cubesat range as a function of time for deployment in the 1.5 revolution stretching direction in the CR3BP are plotted in Fig. 13. First, deployments from the close approach keep-out zone as marked in Fig. 12(a) appear in Fig. 13(a). Note the close approaches, marked by an arrow, that occur approximately 28-30 days after deployment, as predicted by the data in Fig. 10(a). Clearly, these close approaches are unwelcome. Next, appearing in Fig. 13(b) are the deployments in the range 100° < EA < 150° that result in low (blue) values of MI after 55 days in Fig. 12(a). Note the long-duration stays in the NRHO vicinity prior to departure. Finally, cubesats are deployed that avoid both of these undesirable behaviors; their ranges appear in Fig. 12(c). The data in Fig. 10 and Fig. 12 effectively identify favorable deployment options in the CR3BP.

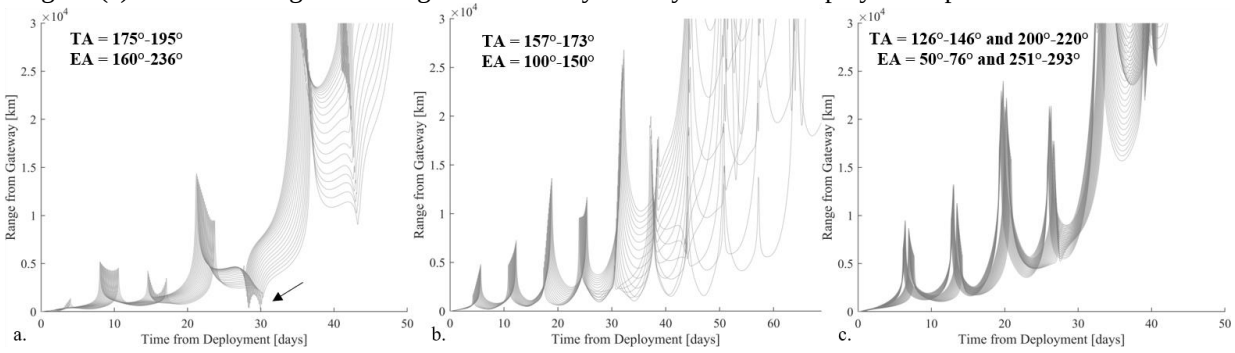


**Fig. 13. Gateway-cubesat range vs. time for three deployment regions with a 1 m/s Δ*v* in a 1.5-revolution stretching direction. Close approach keep-out (a), slow departures (b), and desirable departures (c).**

## VI. Consistency in the Ephemeris Model

Thus far, the CR3BP has been employed to identify behavior patterns across the deployment design space. The same deployment patterns are now assessed in the ephemeris model to ensure consistent behavior across epochs and in the presence of operational errors. First, deployment conditions are sought that ensure consistent, rapid departure across epochs without considering deployment errors. Consider two deployment conditions, each employing a 1.1 m/s Δ*v* in the 1.5-revolution most-stretching direction. The first, with TA = 170° or EA = 141°, commences from a location along the NRHO predicted by the CR3BP analysis to yield slow departures from the NRHO. A cubesat is deployed from this location every revolution for 20 consecutive revolutions along the NRHO, and the resulting Gateway-cubesat range curves appear in Fig. 14(a). The cubesats remain in the NRHO after deployment for up to 94 days; however, the post-deployment duration in the NRHO is inconsistent across the 20 revolutions. In contrast, consider the range plots in Fig. 14(b). In this case, the cubesats are deployed earlier, just after exiting the perilune keep-out zone, at TA = 136° or EA = 61°. Again, one cubesat deployment is simulated per NRHO revolution for 20 consecutive revolutions. This time, however, all of the satellites depart the NRHO within 46 days after deployment; the behavior is consistent across NRHO revolutions in the ephemeris force model. Again, this result agrees with predictions from the CR3BP analysis.

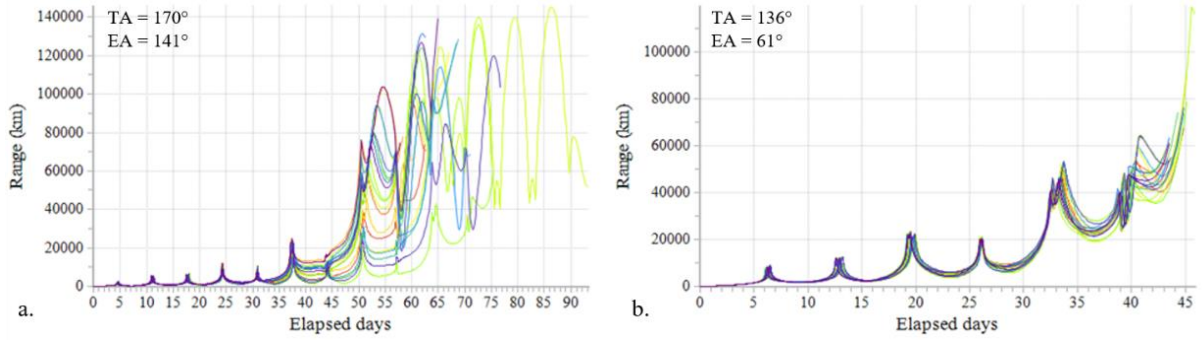


**Fig. 14. Cubesat deployment in the ephemeris model at the same location along the NRHO for 20 consecutive revolutions. TA = 170° (EA = 141°) (a), TA = 136° (EA = 61°) (b).**

To assess the consistency of post-deployment behavior across a year within the Gateway baseline NRHO, deployments are made at a range of magnitudes 0.5 m/s < $\Delta v$ < 1.5 m/s in both the 1.5-revolution and 6.5-revolution time horizon most-stretching directions at 30 locations around the NRHO for 56 consecutive revolutions. The time to depart the NRHO appears as a function of deployment revolution within the NRHO for deployments in the 1.5-revolution stretching direction in Fig. 15. Results from the two deployment locations featured in Fig. 14 appear in Fig. 15(a). Note the long and inconsistent times to depart the NRHO when deployment occurs at TA = 170° (EA = 141°) as compared to results for deployment at TA = 136° (EA = 61°). In Fig. 15(b), 28 additional deployment locations are added. Clearly, some locations along the NRHO yield consistent, fast departures, while others do not. Notable is the blue curve associated with TA = 262° (EA = 328°), which yields the fastest departures dipping below 40 days, but yields inconsistent results.

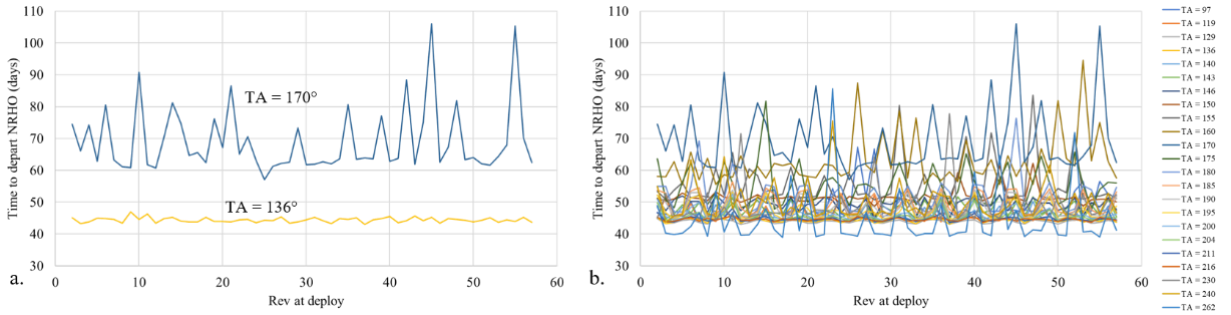


**Fig. 15. Time to depart the NRHO for 56 revolutions along the NRHO. Two deployment locations (a) and 30 deployment locations (b) with a 1.1 m/s $\Delta v$ in the 1.5-revolution most-stretching direction.**

Since inconsistent departure times across the 56 revolutions are associated with a large maximum departure time, the information in Fig. 15 is condensed by recording only the maximum time to depart the NRHO for a given departure location. In this way, departure consistency information for a range of $\Delta v$ magnitudes is reduced to a single plot. The maximum time to depart for deployment maneuvers with magnitudes 0.5 m/s < $\Delta v$ < 1.5 m/s appears as a function of deployment TA in Fig. 16(a) for deployment in the 1.5-revolution stretching direction and in Fig. 16(b) for deployment in the 6.5-revolution stretching direction. Several notable features are apparent. First, note in Fig. 16(a) the large maximum times to depart for deployment locations 155° < TA < 185° (95° < EA < 200°) for all $\Delta v$ magnitudes included in the analysis. These slow departure times are consistent with the CR3BP observations yielded by Fig. 12(a). A similar region of slow departures is not observed in Fig. 16(b), though each individual $\Delta v$ magnitude is associated with slow departures for its own range of TA values. Next, note that there are patterns in the curves for maximum departure time. They do not vary completely randomly; rather, the TA values associated with small maximum departure times change smoothly as $\Delta v$ magnitude changes. Thus, using the data contained in Fig. 16, TA values are identified that consistently lead to fast NRHO departures for a range of $\Delta v$ magnitudes. Note that the variation of departure time as a function of $\Delta v$ magnitude in the ephemeris model is further explored in Davis et al. [4]

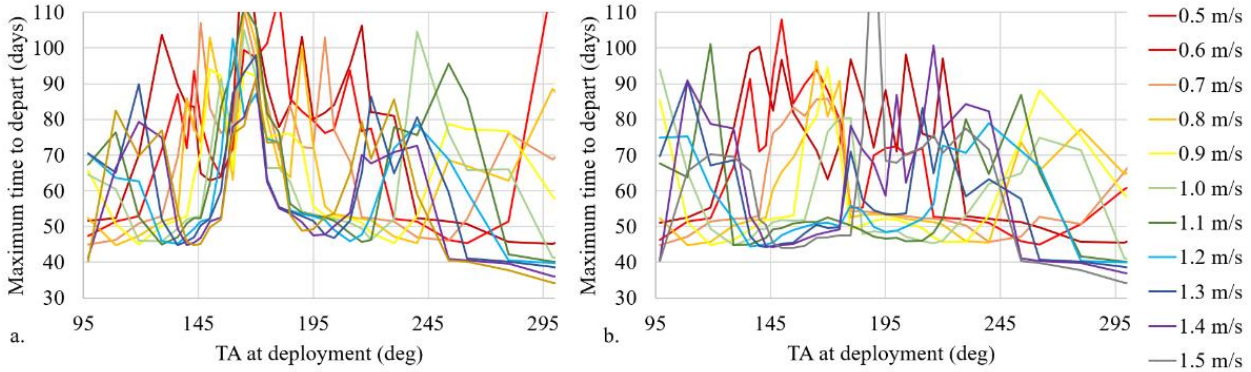


**Fig. 16. Maximum time to depart for deployment locations around the NRHO in the 1.5-revolution stretching direction (a) and the 6.5-revolution stretching direction (b).**

## VII. Cubesat Deployment Green Zones

The goal of the current analysis is the identification of combinations of cubesat deployment locations, directions, and $\Delta v$ magnitudes that yield consistent, fast NRHO departures without conjunctions across epochs and in the presence of operational errors. The CR3BP and ephemeris information detailed thus far is combined to generate candidate green zones for cubesat departure. An example appears in Fig. 17 for deployment prior to apolune in the 1.5-revolution stretching direction. The plot spans deployment locations $120° < TA < 175°$ ($45° < EA < 160°$), or equivalently, the black portion of the NRHO prior to apolune in Fig. 11(a), i.e., the portion not included in the red keep-out zones. This span represents deployment locations along the NRHO that are neither near perilune nor leading to close approaches at subsequent perilune passages; smaller values of TA result in deployment too close to perilune, while larger values of TA result in close Gateway-cubesat conjunctions at subsequent perilune passages. For a subset of $\Delta v$ magnitudes, $1.0 < \Delta v < 1.3$ m/s, the region between TA values of 129° and 146° (equivalently, $53° < EA < 76°$) yields consistent fast departures across 56 revolutions in the NRHO.

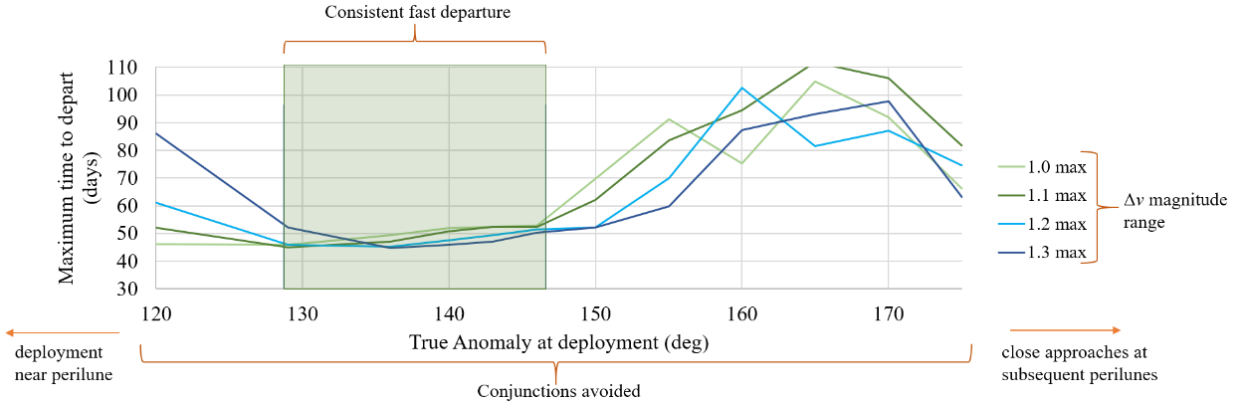


**Fig. 17. Green zone before apolune for deployment in the 1.5-revolution stretching direction.**

The process is repeated to identify candidate green zones in both directions considered in this analysis for deployment before and after apolune. These four candidate green zones appear in Fig. 18. Fig. 18(a) and Fig. 18(c) represent green zones for deployment prior to apolune in the 1.5- and 6.5-revolution stretching directions, respectively. Likewise, Fig. 18(b) and Fig. 18(d) depict green zones for deployment after apolune. Note that the ranges for deployment locations and deployment $\Delta v$ magnitudes differ for the two deployment directions; the $\Delta v$ magnitude range is lower and the deployment location range is shifted to later angles for the 6.5-revolution time horizon as compared to the 1.5-revolution time horizon. Thus, the total green zone is expanded. The larger ranges may enable successful cubesat deployment for a larger range of deployer capabilities and for varying cubesat masses or provide a range for different final destinations to achieve various science, technology, or education objectives. The candidate green zones are summarized in Table 1 and appear overlaid on the Gateway NRHO in Fig. 19; regions along the NRHO included only in a green zone for deployment in the 1.5-revolution stretching direction are marked in light green; portions along the NRHO comprising the green zone only for the 6.5-revolution stretching direction are marked in dark green, and those locations along the NRHO that yield cubesat deployment opportunities in both directions are marked in medium green. Note that these four candidate green zones are not the only possible options for safe cubesat deployment.

**Table 1. Candidate green zones for cubesat deployment: location ranges**

| | Direction | $\Delta v$ range | TA range | EA range | Duration |
|---|---|---|---|---|---|
| before apolune | 1.5 rev stretching | 1.0 - 1.3 m/s | 129-146 deg | 53-76 deg | 6.1 hrs |
| | 6.5 rev stretching | 0.9-1.2 m/s | 129-150 deg | 53-84 deg | 9.0 hrs |
| after apolune | 1.5 rev stretching | 0.8-1.2 m/s | 200-220 deg | 251-293 deg | 18.1 hrs |
| | 6.5 rev stretching | 0.6-0.9 m/s | 215-240 deg | 286-315 deg | 6.9 hrs |

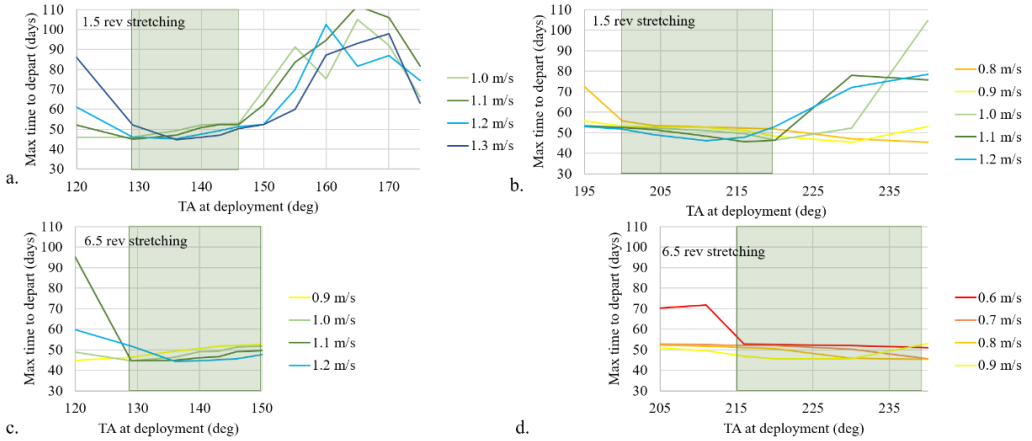


**Fig. 18. Candidate green zones for deployment before (left) and after (right) apolune, in the 1.5-revolution (top) and 6.5-revolution (bottom) most-stretching directions.**

Each of the candidate green zones in Table 1 spans a range of locations along the NRHO along with the associated range of $\Delta v$ magnitudes for deployment. If a single deployment location is selected, successful departure from the NRHO is achievable for a larger range of $\Delta v$ magnitudes beyond those in Table 1. Individual candidate locations along the NRHO are marked in Fig. 19 with asterisks, and each associated $\Delta v$ magnitude range appears in Table 2. The span of $\Delta v$ magnitudes that yield successful deployment for each full TA/EA range in Table 1 is 0.3 – 0.4 m/s. If a single TA/EA is selected as in Table 2, the span of acceptable $\Delta v$ magnitudes increases to 0.4 – 0.6 m/s. Restricting deployment to a single location along the NRHO facilitates successful deployment in the event of larger deployment magnitude errors.

**Table 2. Candidate green zones for cubesat deployment: individual locations**

| | Direction | $\Delta v$ range | TA | EA | Monte Carlo case |
|---|---|---|---|---|---|
| before apolune | 1.5 rev stretching | 0.9-1.3 m/s | 140 deg | 66 deg | A. 1.1 m/s |
| | 6.5 rev stretching | 0.7-1.5 m/s | 140 deg | 66 deg | B. 1.1 m/s |
| after apolune | 1.5 rev stretching | 0.8-1.5 m/s | 200 deg | 251 deg | C. 1.1 m/s |
| | 6.5 rev stretching | 0.6-1.1 m/s | 220 deg | 66 deg | D. 0.8 m/s |

## VIII. Green Zone Limits and Robustness

With candidate green zones identified for ranges of deployment locations along the NRHO, the zones are tested in the ephemeris force model to ensure robustness. First, a deterministic study is conducted in which every deployment opportunity within the proposed green zones is simulated over a year. That is, for deployment both before and after apolune, in both the 1.5-revolution and 6.5-revolution stretching directions, a grid of deployments is executed with 5° steps in osculating true anomaly and 0.1 m/s steps in $\Delta v$ magnitude for the ranges outlined Table 1. The deployments are repeated each revolution for 56 consecutive revolutions, equivalent to 1 year in the NRHO. Operational errors are assumed during Gateway orbit maintenance throughout the simulation, but each deployment maneuver is assumed to take place perfectly, without maneuver execution error of any kind. The results appear colored according to deployment revolution in Fig. 20. In short, each of the cubesat trajectories achieves the momentum integral threshold MI = 0.2 in under 52 days: fast, reliable NRHO departure is achieved for every green zone deployment. Additionally, no close approaches near perilune occur: each deployment exits the NRHO without risk of recontact with the Gateway. Without considering deployment execution errors, the green zones are confirmed for the first year of the Gateway baseline NRHO.

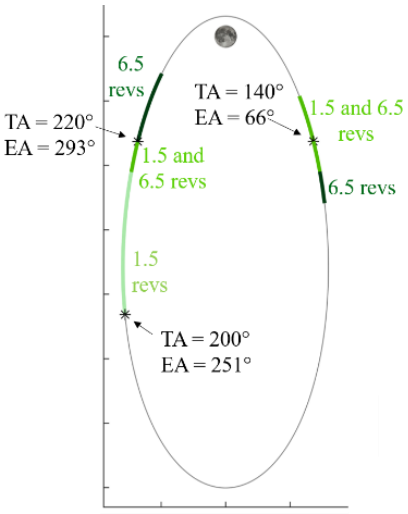


**Fig. 19. Candidate green zones along the NRHO.**

The results in Fig. 20 demonstrate success in the absence of deployment execution errors. In reality, cubesat deployments are often associated with relatively large errors in both magnitude and direction [9]. To investigate the robustness of the candidate green zones, a Monte Carlo analysis is executed to assess the combined effects of errors in $\Delta v$ magnitude and pointing. For this analysis, the NRHO locations specified in Table 2 are employed, and a value

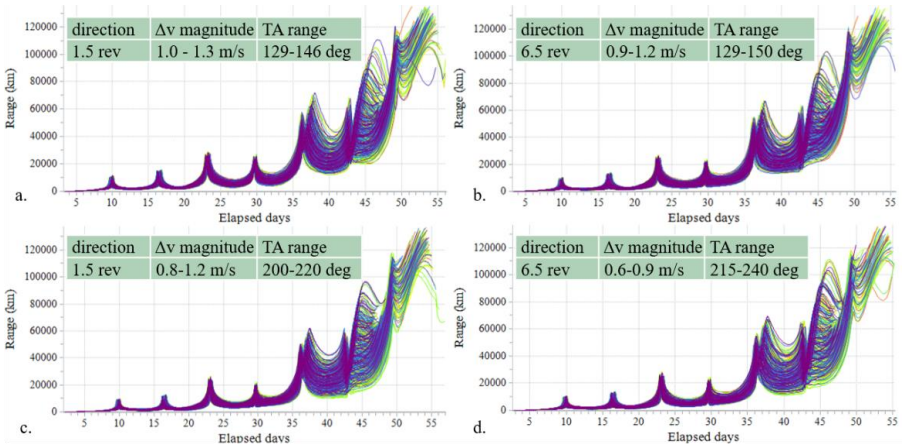


**Fig. 20. Gateway-cubesat range as a function of days past deployment for the candidate green zones over 56 revolutions in the NRHO. Deployment before apolune (top) and after apolune (bottom). No deployment errors incorporated.**

of $\Delta v$ magnitude within each defined range is selected, as indicated in the far-right column of Table 2. Then, errors are applied to the Gateway during orbit maintenance and to the magnitude and direction of cubesat deployment. For each of 9 consecutive revolutions in the NRHO, 100 Monte Carlo trials are executed and each cubesat is propagated until the momentum integral threshold MI = 0.2 is reached, signaling NRHO departure. Thus, a total of 900 Monte Carlo trials are completed for each test. Two levels of deployment execution errors are considered. The first level considers small 3σ deployment errors of 6.67% in magnitude and 1.67° in direction. The second level considers larger deployment errors of 20% in magnitude and 5° in direction (3σ). With both levels of deployment execution errors, orbit determination state errors of 1 km in position and 1 cm/s in velocity (3σ) are assumed at deployment. The green zones are robust to the smaller level of deployment errors; in each of the four cases A-D specified in Table 2, all 900 Monte Carlo trials experience fast, reliable departure without risk of recontact with the Gateway. When the larger deployment execution errors are applied, however, the reliability of the green zones is exceeded. Results appear in Fig. 21 for cases A-D. The plots of Gateway-cubesat range are colored by deployment revolution within the NRHO. In each case, multiple trials exhibit unreliable, slow departure from the NRHO vicinity. One trial in case A (Fig. 21(a)) remains below the MI threshold for 200 days, while the maximum time to depart in the cases B-D is 70-75 days. While no conjunctions with range within 100 km of Gateway are detected, up to 5% of trials fail to depart the NRHO vicinity within 60 days. Thus, the true limit of robustness of the candidate green zones in Table 2 lies between the large and small deployment execution bounds as evaluated in this investigation.

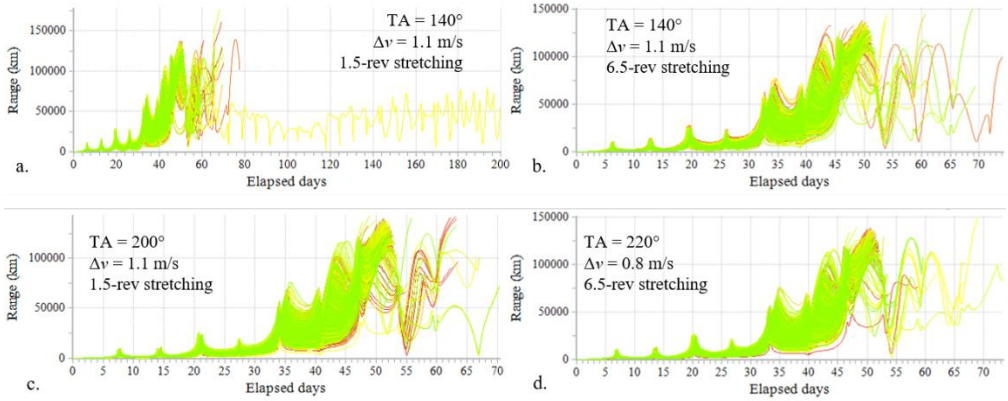


**Fig. 21. Gateway-cubesat range as a function of time past deployment for Monte Carlo cases A-D with large deployment execution errors.**

One important detail of note is the short-term behavior of cubesat trajectories deployed after apolune. At the first perilune passage after deployment, the Gateway-cubesat range briefly decreases prior to resuming its growth. This decrease in range at perilune is observed for all post-apolune deployments investigated in the current study. The results in the CR3BP for deployment across the post-apolune green zone associated with the 1.5-revolution most-stretching direction appear in Fig. 22(a) for a deployment $\Delta v$ of 1 m/s. For deployment at TA = 200° (EA = 251°, marked in orange), the range reaches 120 km before decreasing to approximately 60 km. For later deployments, the time between deployment and perilune passage is shorter, and smaller range values are involved. For deployment at TA = 220° (EA = 293°), for instance, the range reaches a maximum of 30 km, decreases to 20 km, and then resumes growth. Corresponding results in the ephemeris model appear in Fig. 22(b) for 100 Monte Carlo trials for each of 2 revolutions in the baseline NRHO for deployment defined by Monte Carlo case C from Table 2. Because the dip in the range occurs a relatively short time after deployment, the deployment errors of 6.67% in magnitude and 1.67° in direction (3σ) do not have significant time to propagate; the trials all follow a very similar pattern, and while the range does decrease below 100 km, it does so in a predictable fashion and does not represent a threat to the Gateway. Thus, post-apolune departures are not ruled out due to this dip in the range patterns.

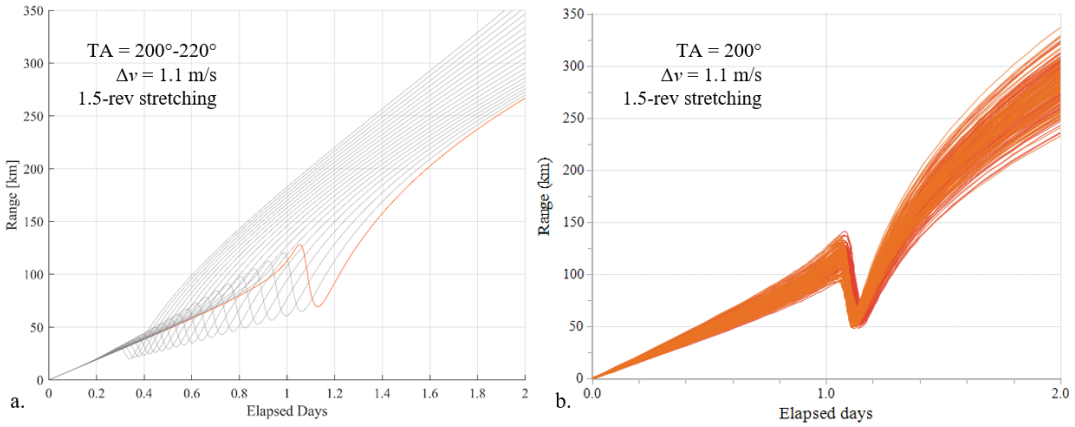


**Fig. 22. Decrease in the Gateway-cubesat range for deployments after apolune in the CR3BP (a) and the ephemeris model (b).**

## IX. Cubesat Recontact Maps

The cubesat trajectory behavior both within and outside of the green zones is also examined in the CR3BP through the use of recontact maps.[6] Recontact maps provide a visual method to quickly assess the risk of recontact or lunar impact for an object separating from the Gateway at a given location and with a particular $\Delta v$ magnitude in any direction. A set of 9 recontact maps appear in Fig. 23. Each map represents deployment from a particular location along the NRHO with a 1 m/s $\Delta v$; deployment from perilune is depicted in Fig. 23(a) and deployment from apolune is illustrated in Fig. 23(f). The various deployment directions are represented by colored points in the map, with yaw along the horizonal axis and pitch on the vertical axis. Thus, each colored point on a map represents deployment from the specified location along the NRHO in a specific direction. Points colored red represent deployment directions that yield a cubesat trajectory that violates a 100 km recontact threshold. Note that the recontact risk for the first ½ revolution in the NRHO is neglected to exclude the range decreases depicted in Fig. 22. Deployment directions that lead to lunar impact are marked in bright yellow; these lunar impacts are rare for $\Delta v$ < 5 m/s [5]. Deployment conditions that lead to NRHO departure without risk of Gateway recontact or lunar impact are marked in shades of blue and green, colored according to time of flight from deployment to NRHO departure, where shades of green represent slower departures and shades of blue denote faster departures. In Fig. 23, the positive most-stretching directions with 1.5-revolution and 6.5-revolution time horizons are marked in black and white, respectively. By design, the black dots, representing deployment in the 1.5-revolution stretching direction, tend to maximize the distance from the red deployment directions that correspond to recontact. Similarly, the white dots, denoting deployment in the 6.5-revolution stretching direction, tends to remain within the darkest blue regions representing the fastest NRHO departures. Note that near perilune in Fig. 23(a), both directions align closely with the velocity direction (yaw = pitch = 0°) and yield fast departures without recontact risk; however, as discussed, the perilune region is excluded due to high sensitivity and operational constraints. Near apolune in Fig. 23(f), red deployment directions that lead to recontact are common. The recontact maps in Fig. 23 yield an immediate visual representation of favorable and unfavorable

deployment opportunities: deployment directions close to red recontact regions are undesirable, while deployment directions represented by deep blue regions in the maps are preferred. These recontact maps also aid in illustrating robustness of the most-stretching directions to perturbations in deployment direction.

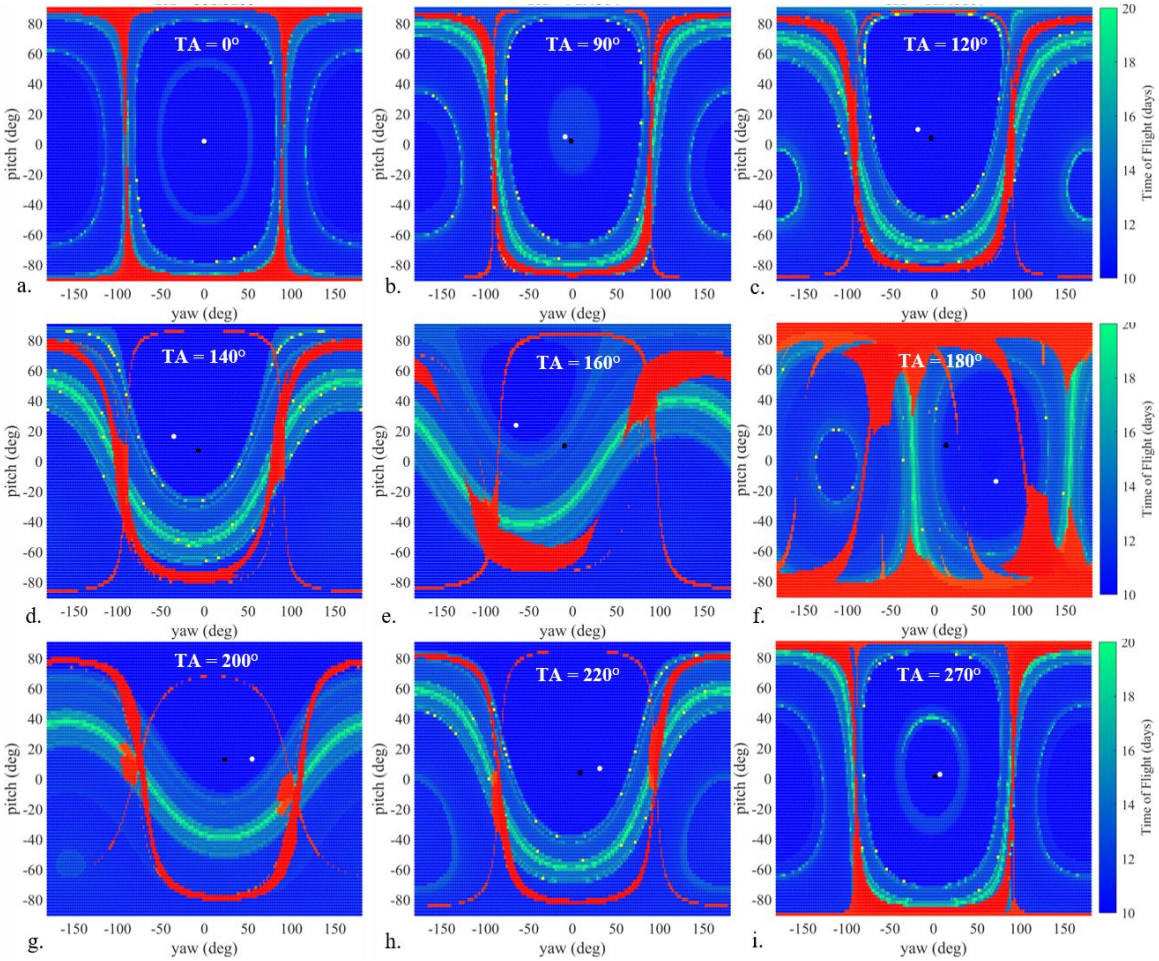


**Fig. 23. Recontact Maps for deployment with $\Delta v$ = 1 m/s.**

## X. Concluding Remarks

The Gateway may provide science, engineering, and educational opportunities via the potential for cubesat deployment from an NRHO. Any cubesat deployed from the Gateway, however, must depart the NRHO vicinity without risk of recontact with the Gateway in the absence of maneuvers after deployment. Because of the nearly stable nature of the NRHO, the lack of atmospheric drag in cislunar space, and the multibody dynamics associated with large cislunar orbits, selecting deployment conditions that yield safe departures is challenging. In this analysis, four candidate green zones are identified that exploit the most-stretching directions along the NRHO to achieve fast, reliable departure from the NRHO via trajectories that avoid reapproaching the Gateway. Cubesat trajectories commencing from these green zones are demonstrated to be robust in the ephemeris model for various epochs in the presence of operational errors.

## Acknowledgments

The authors would like to thank Alexander Hoffman, Stephen Scheuerle, and Kenza Boudad for insightful discussions on this topic. Portions of this work were completed at NASA JSC and Purdue University through contract #NNJ13HA01C and grant #80NSSC18M0122, respectively.

## REFERENCES


[1] Gates, M., M. Barrett, J. Caram, V. Crable, D. Irimies, D. Ludban, D. Manzell, and R. Ticker, "Gateway Power and Propulsion Element Development Status," 69th International Astronautical Congress, Bremen, Germany, October 2018.

[2] Zimovan, E., K. C. Howell, and D. C. Davis, "Near Rectilinear Halo Orbits and Their Application in Cis-Lunar Space," 3rd IAA Conference on Dynamics and Control of Space Systems, Moscow, Russia, May-June 2017.

[3] Boudad, K. K., D. C. Davis, and K. C. Howell, "Disposal Trajectories from Near Rectilinear Halo Orbits," AAS/AIAA Astrodynamics Specialists Conference, Snowbird, Utah, August 2018.

[4] Davis, D.C., K.K. Boudad, S.P. Phillips, and K.C. Howell, "Disposal, Deployment, and Debris in Near Rectilinear Halo Orbits," AAS/AIAA Space Flight Mechanics Meeting, Maui, Hawaii, January 2019.

[5] Davis, D. C., K.K. Boudad, R. J. Power, and K. C. Howell, "Heliocentric Escape and Lunar Impact from Near Rectilinear Halo Orbits," AAS/AIAA Astrodynamics Specialists Conference, Portland, Oregon, August 2019.

[6] Phillips, S. M. and D. C. Davis, "Cloud Computing Methods for Near Rectilinear Halo Orbit Trajectory Design," AAS/AIAA Astrodynamics Specialists Conference, Portland, Oregon, August 2019.

[7] Davis, D. C., R. J. Power, K. C. Howell, and J. P. Gutkowski, "Lunar Impact Probability for Spacecraft in Near Rectilinear Halo Orbits," AAS/AIAA Space Flight Mechanics Meeting, Virtual, January 2021.

[8] Boudad, K. K., K. C. Howell, and D. C. Davis, "Energy and Phasing Considerations for Low-Energy Transfers from Cislunar to Heliocentric Space," AAS/AIAA Space Flight Mechanics Meeting, Virtual, January 2021.

[9] Villela, T, C. A. Costa, A. M. Brandao, F. T. Bueno, and R. Leonardi, "Towards the Thousandth CubeSat: A Statistical Overview," International Journal of Aerospace Engineering, 2019.

[10] Martin-Mur, T. J. and B. Young, "Navigating MarCO, the First Interplanetary CubeSats," 27th International Symposium on Space Flight Dynamics, Melbourne, Australia, February 2019.

[11] Cheetham, B., "Cislunar Autonomous Positioning System Technology Operations and Navigation Experiment (CAPSTONE)," AIAA Ascend Conference, Virtual, November 2020.

[12] McIntosh, Dawn M., J. D. Baker, and J. A. Matus, "The NASA Cubesat missions Flying on Artemis-1," 34th Annual Small Satellite Conference, Virtual, August 2020.

[13] Davis, D. C., F. S. Khoury, and K. C. Howell, "Phase Control and Eclipse Avoidance in Near Rectilinear Halo Orbits," AAS Guidance, Navigation, and Control Conference, Breckenridge, Colorado, February 2020.

[14] Lee, D.E., "Gateway Destination Orbit Model: A Continuous 15 Year NRHO Reference Trajectory," NASA Johnson Space Center White Paper, August 20, 2019.

[15] Guzzetti, D., E. M. Zimovan, K. C. Howell, and D. C. Davis, "Stationkeeping Methodologies for Spacecraft in Lunar Near Rectilinear Halo Orbits," AAS/AIAA Spaceflight Mechanics Meeting, San Antonio, Texas, February 2017.

[16] Muralidharan, V. and K. C. Howell, "Leveraging stretching directions for stationkeeping in Earth-Moon halo orbits," Advances in Space Research, In Press, October 2021.

[17] Davis, D. C., S. A. Bhatt, K. C. Howell, J. W. Jang, R. L. Whitley, F.D. Clark, D. Guzzetti, E. M. Zimovan, and G. H. Barton, "Orbit Maintenance and Navigation of Human Spacecraft at Cislunar Near Rectilinear Halo Orbits," AAS/AIAA Spaceflight Mechanics Meeting, San Antonio, Texas, February 2017.

[18] Newman, C. P., D. C. Davis, R. J. Whitley, J. R. Guinn, and M. S. Ryne, "Stationkeeping, Orbit Determination, and Attitude Control for Spacecraft in Near Rectilinear Halo Orbits," AAS/AIAA Astrodynamics Specialists Conference, Snowbird, Utah, August 2018.

[19] Newman, C. P., J. R. Hollister, F. S. Miguel, D. C. Davis, and D. J. Sweeney, "Attitude Control and Perturbation Analysis of a Crewed Spacecraft with a Lunar Lander in Near Rectilinear Halo Orbit," AAS Guidance, Navigation, and Control Conference, Breckenridge, Colorado, February 2020.